THESIS FOR THE DEGREE OF DOCTOR OF PHILOSOPHY

Investigating the origin of radio emission in nearby starburst galaxies via high-resolution metre and centimetre observations

ESKIL VARENIUS

CHALMERS

Department of Earth and Space Sciences
CHALMERS UNIVERSITY OF TECHNOLOGY
Göteborg, Sweden 2016

Investigating the origin of radio emission in nearby starburst galaxies via high-resolution metre and centimetre observations
ESKIL VARENIUS

ISBN 978-91-7597-476-7
Doktorsavhandlingar vid Chalmers tekniska högskola.
Ny serie nr 4157.
ISSN 0346-718X

Radio Astronomy & Astrophysics Group
Department of Earth and Space Sciences
Chalmers University of Technology
SE–412 96 Göteborg
Sweden
Telephone + 46 (0) 31–772 10 00

Printed by Chalmers Reproservice
Chalmers University of Technology
Göteborg, Sweden 2016

Investigating the origin of radio emission in nearby starburst galaxies via high-resolution metre and centimetre observations

ESKIL VARENIUS
Department of Earth and Space Sciences
Chalmers University of Technology

Abstract

Star formation and galaxy evolution are intimately linked together. A detailed understanding of the physics of star formation can help us explain how galaxies evolve into, for example, our present Milky Way. Using Very Long Baseline Interferometry (VLBI) techniques it is possible to achieve high enough angular resolution to study radio emission from other galaxies in great detail. This thesis presents observations of three nearby Luminous Infrared Galaxies (LIRGs): NGC 4418, M 82 and Arp 220. While the centres of these galaxies are all heavily obscured in optical wavelengths, radio observations can be used to probe star formation properties in the centres of these galaxies.

The galaxy NGC 4418 is radio weak with respect to the far infrared (FIR)-radio correlation for star forming galaxies. We present evidence for a young starburst in the centre, likely fuelled by gas falling in from a recent interaction with the nearby galaxy VV 655. We argue that this scenario can explain the low radio luminosity of this galaxy, and possibly also of other galaxies which appear to be radio weak.

M 82 and Arp 220 follow the FIR-radio correlation and are excellent laboratories to study the physics of star formation in extreme environments. In this thesis we report on new groundbreaking subarcsecond resolution observations of M 82 and Arp 220 with the international LOFAR telescope, where we for the first time spatially resolve the radio emission from their nuclei at metre wavelengths. We report on previously unknown steep-spectrum radio structures and study effects of free-free absorption. We conclude that high angular resolution is essential for a correct interpretation of the radio emission from these complex objects. Furthermore, this work demonstrates that LOFAR can be used to obtain subarcsecond resolution images at metre wavelengths, a capability which can be used in multiple areas of astronomy in the future.

Finally, we present results from new and archival global VLBI observations of Arp 220 spanning 17 years. We show that a self-consistent approach is essential to understand the nature of the radio emission. We find the data rich in details: we detect more than 80 compact objects, many with luminosities and sizes measured at multiple times and frequencies. We present a first analysis of the data where we discuss the general properties of the source population.

Keywords: galaxies: starburst - galaxies: individual: Arp 220, M 82, NGC 4418 - techniques: high angular resolution - stars: supernovae - radio continuum: galaxies

Research contributions

This thesis is based on the work contained in the following five papers:

I. E. Varenius, J. E. Conway, I. Martí-Vidal, S. Aalto, R. Beswick, F. Costagliola, H.-R. Klöckner:
The radio core structure of the luminous infrared galaxy NGC 4418
Astronomy & Astrophysics, 566, 15 (2014).

II. E. Varenius, J. E. Conway, I. Martí-Vidal, R. Beswick, A. T. Deller, O. Wucknitz, N. Jackson, B. Adebahr, M. A. Pérez-Torres, K. T. Chyży, T. D. Carozzi, J. Moldón, S. Aalto, R. Beck, P. Best, R.-J. Dettmar, W. van Driel, G. Brunetti, M. Brüggen, M. Haverkorn, G. Heald, C. Horellou, M. J. Jarvis, L. K. Morabito, G. K. Miley, H. J. A. Röttgering, M. C. Toribio, G. J. White:
Subarcsecond international LOFAR radio images of the M 82 nucleus at 118 MHz and 154 MHz
Astronomy & Astrophysics, 574, 114 (2015).

III. E. Varenius, J. E. Conway, I. Martí-Vidal, S. Aalto, L. Barcos-Muñoz, S. König, M. A. Pérez-Torres, A. T. Deller, J. Moldón, J. S. Gallagher, T. M. Yoast-Hull, C. Horellou, L. K. Morabito, A. Alberdi, N. Jackson, R. Beswick, T. D. Carozzi, O. Wucknitz, N. Ramírez-Olivencia:
Subarcsecond international LOFAR radio images of Arp 220 at 150 MHz. A kpc-scale star forming disk surrounding nuclei with shocked outflows
Accepted for publication in Astronomy & Astrophysics
DOI: 10.1051/0004-6361/201628702

IV. E. Varenius, F. Batejat, J. E. Conway, I. Martí-Vidal, M. A. Pérez-Torres, S. Aalto, A. Alberdi:
The population of SNe/SNRs in the starburst galaxy Arp 220. A self-consistent analysis of 17 years of VLBI monitoring.
Manuscript intended for submission to Astronomy & Astrophysics

V. E. Varenius, F. Costagliola, H.-R. Klöckner, S. Aalto, I. Martí-Vidal, J. E. Conway, H. Spoon:
An atomic hydrogen bridge fueling NGC 4418 with gas from VV 655
Manuscript intended for submission to Astronomy & Astrophysics

I have also contributed to the following publications, not discussed in the thesis:

- L .K. Morabito, J. B. R. Oonk, F. Salgado, M. C. Toribio, H. J. A. Röttgering, A. G. G. M. Tielens, R. Beck, B. Adebahr, P. Best, R. Beswick, A. Bonafede, G. Brunetti, M. Brüggen, K. T. Chyży, J. E. Conway, W. van Driel, J. Gregson, M. Haverkorn, G. Heald, C. Horellou, A. Horneffer, M. Iacobelli, M. J. Jarvis, I. Marti-Vidal, G. Miley, D. D. Mulcahy, E. Orrú, R. Pizzo, A. M. M. Scaife, **E. Varenius**, R. J. van Weeren, G. J. White, M. W. Wise:
Discovery of Carbon Radio Recombination Lines in M82
The Astrophysical Journal Letters, 795, 33 (2014)

- N. Ramírez-Olivencia, **E. Varenius**, M. A. Pérez-Torres, J. Conway, A. Alberdi, R. Herrero-Illana:
EVN imaging of the LIRGI sample
Highlights of Spanish Astrophysics VIII, Proceedings of the XI Scientific Meeting of the Spanish Astronomical Society held on September 8-12, 2014, in Teruel, Spain, ISBN 978-84-606-8760-3 (2015)

- J. Moldón, A. T. Deller, O. Wucknitz, N. Jackson, A. Drabent, T. Carozzi, J. Conway, A. D. Kapińska, J. P. McKean, L. Morabito, **E. Varenius**, and 74 additional coauthors:
The LOFAR long baseline snapshot calibrator survey
Astronomy & Astrophysics, 574, 73 (2015)

- G .H. Heald, R. F. Pizzo, E. Orrú, R. P. Breton, D. Carbone, C. Ferrari, M. J. Hardcastle, W. Jurusik, G. Macario, D. Mulcahy, D. Rafferty, A. Asgekar, M. Brentjens, R. A. Fallows, W. Frieswijk, M. C. Toribio, B. Adebahr, M. Arts, M. R. Bell, A. Bonafede, J. Bray, J. Broderick, T. Cantwell, P. Carroll, U. Cendes, A. O. Clarke, J. Croston, S. Daiboo, F. de Gasperin, J. Gregson, J. Harwood, T. Hassall, V. Heesen, A. Horneffer, A. J. van der Horst, M. Iacobelli, V. Jelić, D. Jones, D. Kant, G. Kokotanekov, P. Martin, J. P. McKean, L. K. Morabito, B. Nikiel-Wroczyński, A. Offringa, V. N. Pandey, M. Pandey-Pommier, M. Pietka, L. Pratley, C. Riseley, A. Rowlinson, J. Sabater, A. M. M. Scaife, L. H. A. Scheers, K. Sendlinger, A. Shulevski, M. Sipior, C. Sobey, A. J. Stewart, A. Stroe, J. Swinbank, C. Tasse, J. Trüstedt, J.; **E. Varenius**, and 86 additional coauthors:
The LOFAR Multifrequency Snapshot Sky Survey (MSSS). I. Survey description and first results
Astronomy & Astrophysics, 582, 123 (2015)

- R. Amanullah, J. Johansson, A. Goobar, R. Ferretti, S. Papadogiannakis, T. Petrushevska, P. J. Brown, Y. Cao, C. Contreras, H. Dahle, N. Elias-Rosa, J. P. U. Fynbo, J. Gorosabel, L. Guaita, L. Hangard, D. A. Howell, E. Y. Hsiao, E. Kankare, M. Kasliwal, G. Leloudas, P. Lundqvist, S. Mattila, P. Nugent, M. M. Phillips, A. Sandberg, V. Stanishev, M. Sullivan, F. Taddia, G. Östlin, S. Asadi, R. Herrero-Illana, J. J. Jensen, K. Karhunen, S. Lazarevic, **E. Varenius**, P. Santos, S. S. Sridhar, S. H. J. Wallström, J. Wiegert:
Diversity in extinction laws of Type Ia supernovae measured between 0.2 and 2 μm
Monthly Notices of the Royal Astronomical Society, 435, 3300 (2015)

- L. K. Morabito, A. T. Deller, H. Röttgering, G. Miley, **E. Varenius**, T. W. Shimwell, J. Moldón, N. Jackson, R. Morganti, R. J. van Weeren, J. B. R. Oonk:
LOFAR VLBI Studies at 55 MHz of 4C 43.15, a z=2.4 Radio Galaxy
Monthly Notices of the Royal Astronomical Society, 461, 2676 (2016)

- T. Hobiger, R. Haas, **E. Varenius**:
Hard- and software tools for the education of geodetic VLBI
IVS 2016 General Meeting Proceedings "New Horizons with VGOS", in print.

- N. Jackson, A. Tagore, A. T. Deller, J. Moldón, **E. Varenius**, and 74 additional coauthors: *LBCS: the LOFAR Long-Baseline Calibrator Survey*
Accepted for publication in Astronomy & Astrophysics. (arXiv:1608.02133)

- T. W. Shimwell, H. J. A. Röttgering, P. N. Best, W. L. Williams, T.J. Dijkema, F. de Gasperin, M. J. Hardcastle, G. H. Heald, D. N. Hoang, A. Horneffer, H. Intema, E. K. Mahony, S. Mandal, A. P. Mechev, L. Morabito, J. B. R. Oonk, D. Rafferty, E. Retana-Montenegro, J. Sabater, C. Tasse , R. J. van Weeren, M. Brüggen, G. Brunetti, K. T. Chyży, J. E. Conway, M. Haverkorn, N. Jackson, M. J. Jarvis, J. P. McKean, G. K. Miley, R. Morganti, G. J. White, M. W. Wise, I. M. van Bemmel, R. Beck, M. Brienza, A. Bonafede, G. Calistro Rivera, R. Cassano, A. O. Clarke, D. Cseh, A. Deller, A. Drabent, W. van Driel, D. Engels, H. Falcke, C. Ferrari, S. Fröhlich, M. A. Garrett, J. J. Harwood, V. Heesen, M. Hoeft, C. Horellou, F. P. Israel, A. D. Kapińska, M. Kunert-Bajraszewska, D. J. McKay, N. R. Mohan, E. Orru, R. F. Pizzo, I. Prandoni, D. J. Schwarz, A. Shulevski, M. Sipior, D. J. B. Smith, S. S. Sridhar, M. Steinmetz, A. Stroe, **E. Varenius**, P. P. van der Werf, J. A. Zensus, J. T. L. Zwart:
The LOFAR Two-metre Sky Survey – I. Survey Description and Preliminary Data Release
Submitted to Astronomy & Astrophysics.

Acknowledgements

Five years would have been much too short for me to do this work all by myself. Luckily I have been surrounded by good people who have given me a lot of support in many different ways.
First and foremost, I want to extend my gratitude towards my three supervisors. I want to thank John Conway for accepting me as a PhD candidate, for kindly proving me wrong when I was wrong, and for giving me due credit when I was right. You made me feel like a researcher from the start. I want to thank Iván Martí-Vidal for your unlimited enthusiasm and technical brilliance. You are the most powerful Parselmouth I have met, and the observatory is lucky to have you. Last but not least, I want to thank Susanne Aalto for always believing in me, for introducing me to galaxies in all shapes and forms, and for many interesting discussions about leadership and science. I hope we can continue our discussions for many years to come.
To all my colleagues and friends in Onsala and around the world: the work in this thesis could not have been done without all your good feedback, encouragement and laughs. Thank you! In particular, I want to thank Cathy Horrelou, who first opened my eyes to radio astronomy and public outreach by introducing me to SALSA, Simon Casey, for patiently sorting out numerous computer issues which could have stopped this thesis work many times, and Adriene Mishler for your wonderful online yoga class library which made me not only survive but also smile as I wrote the last parts of this thesis.
I want to thank my parents, my two sisters, and my love Hanna for all your support during these, sometimes long, five years. You inspire me to continue forward and to remember the joy of music. I love you all!
Finally, I want to acknowledge the large amount of luck without which this thesis would never have been written. I have, for example, been very lucky to grow up in a country with free education, good health care and no wars. Elsewhere, I may never have learned basic physics, my broken foot in eight grade may have left me disabled, and I may have been forced to flee to save my life. I hope that some day, luck will play a smaller role so that everyone who wants to spend their time pondering the wonders of nature will be given the opportunity to do so.

Eskil

Contents

Abstract i
Research contributions iii
Acknowledgements vi

1 Introduction **1**
1.1 Outline of this thesis 2
1.2 Radio emission from star forming galaxies 2
1.2.1 Free-free emission and absorption 4
1.2.2 Synchrotron emission and absorption 4
1.3 The FIR-radio correlation 5
1.3.1 A more elaborate model of the FIR-radio correlation 6
1.4 Telescopes used in this work 8
1.4.1 The Karl G. Jansky Very Large Array (VLA) 8
1.4.2 The Multi-Element Radio Linked Interferometer Network (e-MERLIN) 9
1.4.3 Global Very Long Baseline Interferometry (VLBI) 9
1.4.4 The LOw Frequency ARray (LOFAR) 9

2 Calibration of interferometric data **11**
2.1 Long baseline interferometry 11
2.2 The small field-of-view approximation 12
2.2.1 Time and frequency smearing 13
2.3 Phase-referencing 14
2.3.1 Phase-referencing in cm-VLBI 14
2.3.2 Phase-referencing in metre-VLBI with LOFAR 15
2.4 Flux density calibration 15
2.4.1 Flux density calibration in global VLBI 16
2.4.2 Flux density calibration in metre-VLBI with LOFAR 16

3 Summary of appended papers **19**
3.1 Introduction to paper I: What is powering NGC 4418? 19
3.1.1 Summary of paper I 21
3.1.2 Follow-up work 22
3.2 Introduction to paper II: Subarcsecond imaging of M 82 with LOFAR . . 22

3.2.1 Summary of paper II . . . 23
3.2.2 Follow-up work . . . 24
3.3 Introduction to paper III: Subarcsecond imaging of Arp 220 with LOFAR 24
3.3.1 Summary of paper III . . . 25
3.3.2 Follow-up work . . . 26
3.4 Introduction to paper IV: 17 years of VLBI monitoring of Arp 220 . . . 26
3.4.1 Summary of paper IV . . . 27
3.4.2 Follow-up work . . . 27
3.5 Introduction to paper V: An atomic hydrogen bridge fueling NGC 4418 . 28
3.5.1 Neutral hydrogen (HI) emission and absorption . . . 29
3.5.2 Summary of paper V . . . 29
3.5.3 Follow-up work . . . 29

4 Summary and outlook **31**

Bibliography **33**

Acronyms **37**

Appendices **39**

A Time and frequency smearing **41**
A.1 Averaging of plane waves in Fourier space . . . 41
A.2 Frequency smearing . . . 42
A.3 Time smearing . . . 42
A.4 Coherence loss due to residual delays and rates . . . 43

Paper I **45**

Paper II **55**

Paper III **73**

Paper IV **93**

Paper V **119**

Chapter 1

Introduction

Observations of distant stars and galaxies provide an important way to learn more about ourselves and the world around us. In the past century we have, for example, learned that iron, which is important for oxygen transport in our blood, is created in massive stars and released into space in supernova explosions. We have also learned that although there are planets around many other stars, the Earth is a unique place which we should care about if we want future generations to be able to enjoy it as much as we do.

Although many useful discoveries and inventions arise from knowledge driven research[1], there is great value in pursuing knowledge simply because one is curious. In this thesis we have been curious about radio emission from star forming galaxies, and tried to learn more about its origins. This work touches upon many areas, from supernova explosion physics to data management and modelling. We have, for example, figured out how to make very sharp images of the sky at very long radio waves using the international Low Frequency ARray (LOFAR; van Haarlem et al. 2013).

A new telescope such as LOFAR opens up a new window towards the universe. Already today astronomers have access to vast amounts of data (e.g. images) of stars, galaxies and other things visible in the sky. LOFAR has ambitious goals for surveying the sky, as has the next generation radio telescope, the Square Kilometre Array (SKA). Because of the large number of sources in surveys of the sky (e.g. $\sim 200\,000$ in the LOFAR Multifrequency Snapshot Sky Survey (MSSS); Heald et al. 2015), statistical methods studying populations of e.g. galaxies will likely dominate future analysis work, compared to efforts focusing on single interesting objects. These methods often make use of empirical (or theoretical) relations between e.g. the measured luminosity of a galaxy in radio waves and the number of stars formed (on average) by this galaxy every year.

While such relations have been observationally established at GHz frequen-

[1] For example, MRI and CT cameras, today routinely used in hospitals around the world, build on the *Projection-slice theorem* first presented by Bracewell (1956) in the context of Radio Astronomy.

cies, the validity at lower frequencies probed by LOFAR (and the SKA) remains to be checked observationally. For example, a FIR-radio correlation (see Sect. 1.3) may exist at other frequencies than 1.4 GHz although with increased non-linearity (e.g. Fig. 10 by Lacki et al. 2010). The reliability of star formation rate estimates based on observations of galaxies at MHz frequencies can likely be improved by detailed studies of a few objects which are relatively well understood throughout the electromagnetic spectrum, such as the galaxies Arp 220 and M 82 which are described in this thesis.
The field of star formation covers many scales, from the formation and evolution of single stars to the feedback by the stellar population on galaxy evolution (Kennicutt & Evans 2012). In this work we study radio emission from star formation on scales from a tenth of a parsec up to several kiloparsec using radio astronomical interferometry at metre and centimetre wavelengths. The main aim is to improve our understanding of the origin of the observed radio emission. The work presented on metre wavelengths makes use of the new international LOFAR telescope, and a significant part of this thesis work has been to develop strategies for how to make images of the sky at metre wavelengths using the full resolution power of LOFAR.
In this work, we have mainly studied radio continuum emission. In addition to the continuum, there are many spectral lines present at radio frequencies which carry a wealth of interesting information. While this thesis focuses on radio continuum, a brief introduction to the 21 cm hydrogen line is included as part of the introduction to paper V.

1.1 Outline of this thesis

This thesis is structured as follows. The rest of this introductory chapter provides a brief summary of a few key aspects of radio emission from star forming galaxies. Chapter 2 summarises the calibration strategies used in this work, in particular regarding how to analyse data from the international LOFAR telescope. Chapter 3 introduces the five appended papers, and finally chapter 4 summarises the main conclusions of this thesis.

1.2 Radio emission from star forming galaxies

General reference: Condon (1992)
The observed radio continuum of a star forming galaxy is a combination of emission and absorption of photons by charged particles moving in electromagnetic fields. Two very important processes give rise to what is usually referred to as respectively free-free emission (Sect. 1.2.1) and synchrotron emission (Sect. 1.2.2). A simple model combining free-free emission, absorption and

synchrotron emission from was used in paper I, to estimate the star formation rate of compact features in the nucleus of the galaxy NGC 4418, and in paper III to model the radio emission from the nuclei of Arp 220. For shorter wavelengths, i.e. at submillimetre wavelengths and the far-infrared, emission from dust grains dominate the spectrum. The different contributions from free-free, synchrotron and dust can be seen as a function of frequency in Fig. 1.1 for the starburst galaxy M 82.

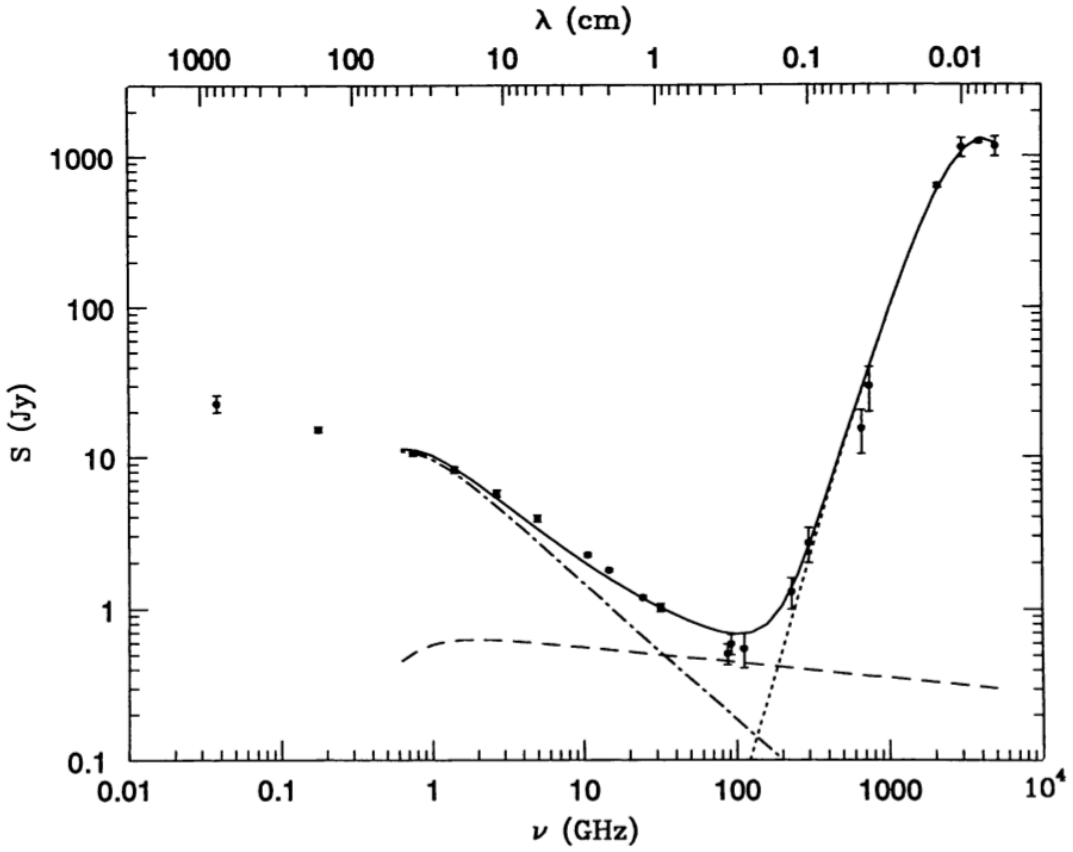

Figure 1.1: The observed spectrum of M 82 from radio to FIR wavelengths, is the sum (solid line) of synchrotron (dot-dash line), free-free (dashed line) and dust (dotted line) components. The HII regions in this bright starburst galaxy start to become opaque below $\nu \sim 1$ GHz, reducing both the free-free and synchrotron flux densities. Thermal re-radiation from dust swamps the radio emission at higher frequencies. Figure from Condon (1992).

1.2.1 Free-free emission and absorption

Free-free emission is produced in electromagnetic interactions between charged particles such as electrons or protons. The term free-free refers to that the particles are not bound in atoms before and after the interaction. Free-free emission is sometimes also referred to as *Brehmsstrahlung* because deceleration means "to brake", or as *thermal* emission, because the distribution of kinetic energies of the charged particles can be described by a Boltzmann distribution with some temperature. The frequency dependence of the free-free emission at optically thin frequencies can be described by a power-law $S_\nu \propto \nu^{-0.1}$ (see the dashed line in Fig. 1.1).
The free particles involved in producing the emission are usually created from ionisation of atoms or molecules close to a strong radiation source, such as a massive star or an accreting black hole. If the free-free emission is due to star formation, it is a direct measure of the current number of the most massive (and short-lived) stars. These stars emit many photons energetic enough ($h\nu > 13.6eV$) to ionise a large volume of the atomic hydrogen present in the circumstellar medium (CSM). Such an ionised region is called an HII-region and may be observable at radio wavelengths.
The inverse mechanism, called free-free *absorption*, means that instead of emitting a photon as a result of the interaction, a photon is absorbed and the energy transferred to the charged particles involved. This effect is very significant at low frequencies and can attenuate any background radio emission, thereby flattening the radio spectra (below 1 GHz in Fig. 1.1). An optically thick HII region can be described as a black body with some temperature, i.e. the spectrum is described by the power-law $S_\nu \propto \nu^2$ at frequencies where the Rayleigh-Jeans approximation is valid.

1.2.2 Synchrotron emission and absorption

Synchrotron emission comes from relativistic charged particles moving in a magnetic field, see Fig. 1.2. In star forming galaxies, synchrotron emission from electrons and positrons accelerated in supernova remnants dominates the radio spectrum at GHz frequencies, although it is attenuated by free-free absorption at the lowest frequencies. The spectrum of (unabsorbed) synchrotron emission can be described by the power-law $S_\nu \propto \nu^\alpha$ (see Fig. 1.1). The power-law index α depends on the distribution of energies in the ensemble of emitting particles and is usually observed to be close to -0.8. Since the particles lose energy as radiation, they will eventually stop emitting if new energy (or new particles) is not injected. More energetic particles lose their energy quicker, leading to a steepening of the radio spectrum at higher frequencies. This effect is called synchrotron ageing and may be used to estimate the age of an ensemble of emitting particles.

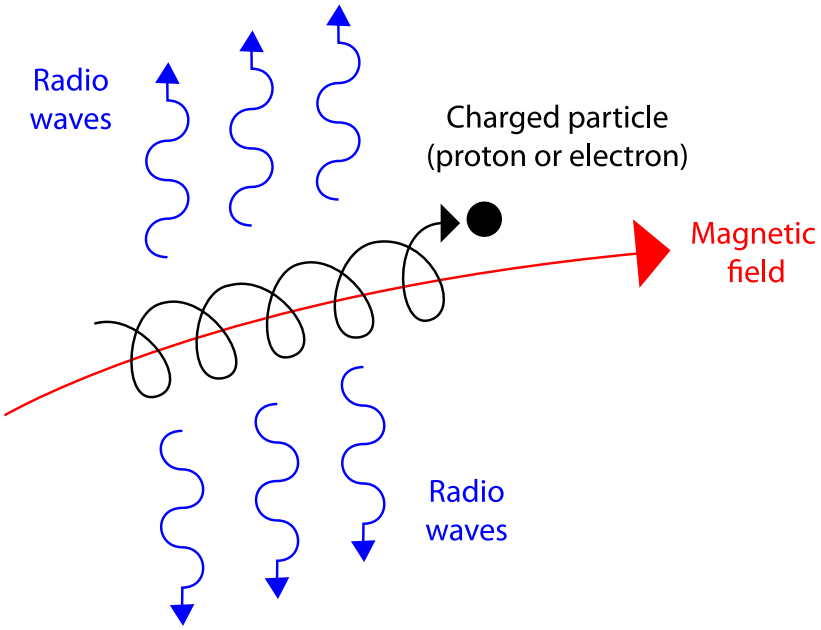

Figure 1.2: Charged particles spinning around magnetic field lines produce synchrotron radiation. Synchrotron radiation observed at radio wavelengths allow us to study astrophysical phenomena such as supernovae in detail. Image credit: High-resolution version by Simon Farsi, original at http://nrumiano.free.fr/PagesU/Elexique.html.

The inverse process is also possible, i.e. that a charged particle in a magnetic field absorbs a photon. This is called synchrotron absorption, but is only significant in extremely bright objects, where the major part of the radio emission is usually synchrotron radiation. Therefore, the absorption process is usually referred to as synchrotron self-absorption (SSA).

1.3 The FIR-radio correlation

There is a strong observed relation between the luminosity of a galaxy at radio and at infrared wavelengths, see Fig. 1.3, and this is often referred to as the FIR-radio correlation. The correlation between the two wavebands is usually explained by star formation being the ultimate source of emission in both wavebands. The infrared emission is thought to come from dust grains which absorb UV-light from stars and re-emit the energy in the infrared where it then escapes the galaxy. The radio emission is thought to be dominated by synchrotron radiation from relativistic electrons accelerated in supernova remnants.
It has been proposed that the FIR-radio correlation can be used to separate star

forming galaxies from active galaxies (AGNs, hosts of highly-accreting supermassive black holes), and could therefore be used as a tool to find galaxies powered by AGN emission. However, the correlation is also interesting to study in itself because of the tight connection to the physics of star formation in a wide range of environments.
The correlation is usually described in terms of a logarithmic ratio , q, between flux densities at FIR and radio wavelengths:

$$q \equiv \log\left(\frac{\mathrm{FIR}}{3.75\times10^{12}\mathrm{Wm}^{-2}}\right) - \log\left(\frac{S_{1.4\mathrm{GHz}}}{\mathrm{Wm}^{-2}\mathrm{Hz}^{-1}}\right) \tag{1.1}$$

where $S_{1.4\mathrm{GHz}}$ is the observed 1.4 GHz flux density in units of $\mathrm{Wm}^{-2}\mathrm{Hz}^{-1}$ and

$$\mathrm{FIR} \equiv 1.26\times10^{-14}(2.58S_{60\mu m} + S_{100\mu m}) \tag{1.2}$$

where $S_{60\mu m}$ and $S_{100\mu m}$ are the flux densities (in Jy) measured in the 60 and 100 μm bands with the Infrared Astronomical Satellite (IRAS) (Yun et al. 2001). A large value of q means little radio emission in relation to FIR. The relation is remarkably tight over several orders of magnitude in luminosity, see Fig. 1.3, with an average value of $q = 2.34$. Very few galaxies differ significantly from the observed correlation. Yun et al. (2001) find only nine objects of 1809 with $q \geq 3$, i.e. showing significantly less radio emission than expected given their FIR luminosity. One of these galaxies is NGC 4418 which is discussed in papers I and V in this thesis.

1.3.1 A more elaborate model of the FIR-radio correlation

The wide range of properties of galaxies following the FIR-radio correlation has inspired studies trying to explain the physics behind this relation in detail. A simple calorimeter model where all UV light is re-radiated as infra-red and all relativistic electrons radiate their energy as synchrotron emission, is probably not true. For example, Lacki et al. (2010) argue that since most normal galaxies show a significant UV luminosity, not all UV is absorbed by dust. Also, if the electrons lost all their energy before leaving the galaxy the spectral index α would be around -1, but instead it is ~ -0.8 as mentioned above. Therefore, a fraction of charged particles must leave the galaxies before radiating all their energy. These effects may be said to *conspire* to give rise to the observed correlation for normal galaxies.
For low surface density galaxies, Lacki et al. (2010) argue that a significant fraction of charged particles escape the galaxy before loosing their energy as synchrotron radiation, and these galaxies would therefore appear relatively weak at radio wavelengths. However, these galaxies are also less dusty, thereby decreasing the UV-opacity which decreases the FIR luminosity. Once again, the effects conspire to produce the correlation also for low density environments.

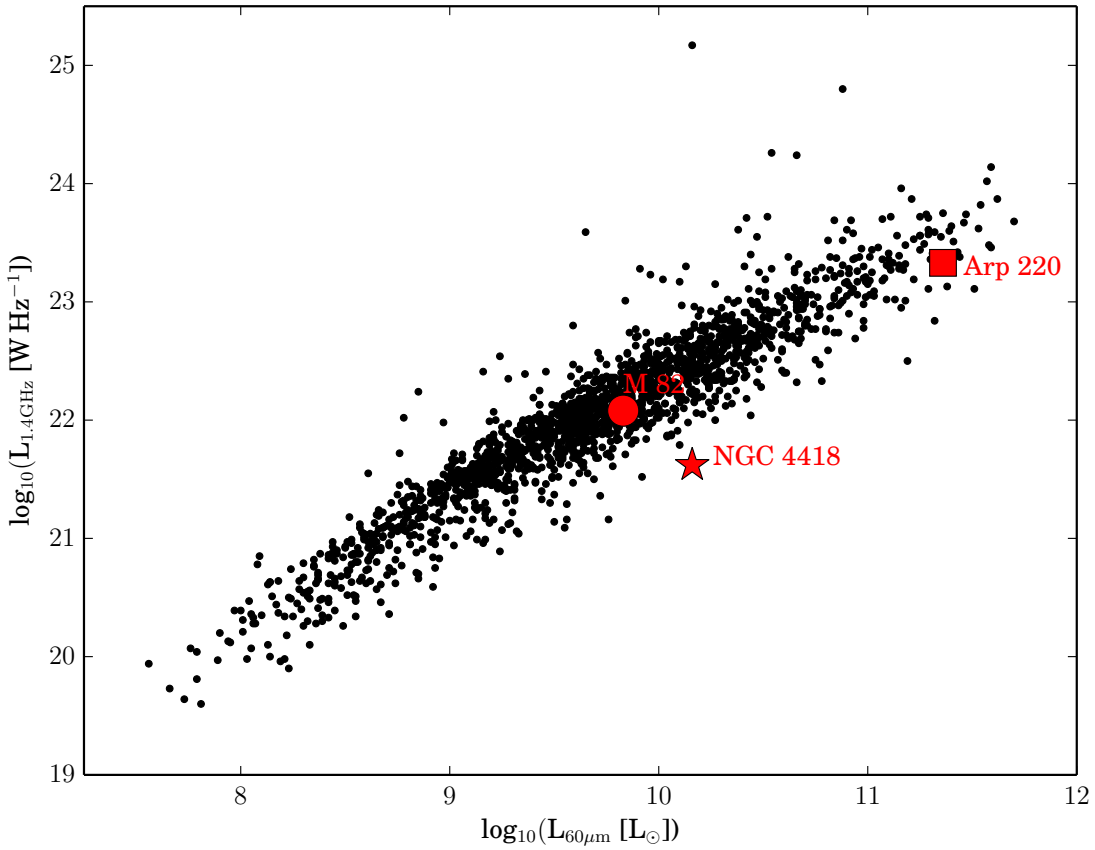

Figure 1.3: 1.4 GHz radio luminosity vs infrared 60 μm luminosity using data from Yun et al. (2001), i.e. a remake of their Fig. 5a. The three galaxies studied in this thesis are marked in red: NGC 4418 as a star, M 82 as a circle and Arp 220 as a square.

In dense starburst galaxies, high-energy protons (and atomic nuclei) accelerated by SNe are important for the energy balance, in addition to the $e^{\pm}$ which emit the observed synchrotron radiation. Collisions between relativistic protons from SNe and protons in the interstellar medium (ISM) produce pions, which decay into gamma rays, neutrinos and *secondary* $e^{\pm}$, in addition to the *primary* $e^{\pm}$ injected directly by SNe. Lacki et al. (2010) argue that secondary electrons and positrons likely are comparable to, or dominate, primary electrons in dense star bursts. However, the increased number of relativistic particles that could produce more synchrotron radiation is compensated for by more significant inverse Compton scattering and ionisation losses in regions with strong radiation from massive stars and dense atomic and molecular gas. Again, although for different reasons than in lower density environments, one expects the FIR-radio correlation to hold also for very dense starbursts.

To learn more about the physics of star formation, and to test models of the FIR-radio correlation, such as presented by Lacki et al. (2010), we can study nearby starburst galaxies where the main sources of particle acceleration, i.e. the SNe/SNRs (and possibly AGNs) can be studied in detail. Two starburst galaxies on the FIR-radio correlation are M82 and Arp 220.
M 82 is relatively nearby (3.6 Mpc) and has been well studied across the electromagnetic spectrum, although observations with high-angular resolution have been lacking at metre wavelengths where e.g. free-free absorption is most prominent. Arp 220 is more distant (77 Mpc) but has a star formation rate (SFR) of more than $100\,\mathrm{M}_\odot\,\mathrm{yr}^{-1}$ (Bressan et al. 2002), i.e. two orders of magnitude higher than the $\sim 1\,\mathrm{M}_\odot\,\mathrm{yr}^{-1}$ of the present Milky Way (Robitaille & Whitney 2010) and among the highest in the nearby ($z < 0.1$) universe (Salim et al. 2007). With a large number of SNe/SNRs evolving in a very high density environment (Batejat et al. 2011), it is a good laboratory for studies of star formation in extreme environments.
Important clues about the physics of the FIR-radio correlation may also be found from studying the few galaxies not following the correlation, such as the galaxy NGC 4418. In this thesis we study these three, quite different, galaxies: NGC 4418, M 82, and Arp 220 using multiple radio telescopes observing at metre and centimetre wavelengths.

1.4 Telescopes used in this work

In this thesis we use data from multiple radio interferometers, i.e. arrays of connected radio telescopes. Interferometers are widely used because of their ability to produce images of the sky with high angular resolution. The angular resolution θ in radians of an interferometer can be approximately described (similarly to a single dish telescope) as $\theta \approx \lambda/D$, where λ is the observing wavelength and D is the largest separation possible between the telescopes included in the array. This section provides a brief overview of the interferometers used in this work.

1.4.1 The Karl G. Jansky Very Large Array (VLA)

The VLA is an interferometer in New Mexico (U.S.A) which can observe radio emission at MHz and GHz frequencies. The antennas are movable and are used in four different configurations to sample the sky at different spatial scales[2], covering a range of antenna separations from 35 m to 36.4 km. For example: at 6 GHz in its most extended configuration, the array can sample emission on scales smaller than $8.9''$ with a maximum resolution of $0.33''$. In this work, the VLA is used in paper III to study the radio emission from the centre of the

[2]For all capabilities see https://science.nrao.edu/facilities/vla.

galaxy Arp 220 at 1.4 GHz, 6 GHz and 33 GHz, and in paper V to study radio continuum and HI-line emission from NGC 4418 at 1.4 GHz.

1.4.2 The Multi-Element Radio Linked Interferometer Network (e-MERLIN)

The e-MERLIN array (or MERLIN as it was called before the last major upgrade) is an interferometer in the United Kingdom. It consists of seven telescopes with a maximum separation of 217 km, giving an angular resolution of about 40 milliarcseconds at 5 GHz, i.e. comparable to the Hubble Space Telescope. e-MERLIN samples a range of spatial scales between those sampled by the VLA (Sect. 1.4.1) and global VLBI (Sect. 1.4.3). Papers I and III in this thesis make use of data from the MERLIN and paper II from the new e-MERLIN.

1.4.3 Global Very Long Baseline Interferometry (VLBI)

Global VLBI offers the highest possible angular resolution by combining data from telescopes spread all over the Earth. In this work we have used data from the European VLBI Network (EVN) and the Very Long Baseline Array (VLBA) in the U.S.A. to probe angular scales of less than 1 milliarcsecond. Data from the EVN is used in paper I to probe the structure of radio emission in the centre of the galaxy NGC 4418, and in paper IV multiple observing epochs, of both the VLBA and the EVN, are used to study the origins of radio emission in the galaxy Arp 220. While global VLBI offers unique capabilities in terms of e.g. image resolution, there are also challenges such as optimal scheduling of telescopes which do not see the same part of the sky, correcting for differences in telescope clocks, or being able to combine the data from telescopes with very different specifications (such as sensitivity) to make deep images. Still, global VLBI makes it possible to make very detailed studies of relatively compact celestial objects, such as supernovae, at GHz frequencies.

1.4.4 The LOw Frequency ARray (LOFAR)

The international LOFAR telescope is a fairly new telescope built to observe radio waves of MHz frequencies (van Haarlem et al. 2013). The Swedish LOFAR station in Onsala was inaugurated in September 2011, just a few days after I started my PhD education. Today LOFAR consists of 50 stations in six countries, and another station is currently being constructed in Ireland, see Fig. 1.4.
The LOFAR telescope has many aims and science goals, from studies of pulsars and high-energy particle physics to studies of galaxy evolution and the epoch of reionization. It is in many ways a software-defined telescope, constructed without moving parts, in contrast to the mechanically tracking dishes which make up the VLA. This new software based telescope provides exciting new

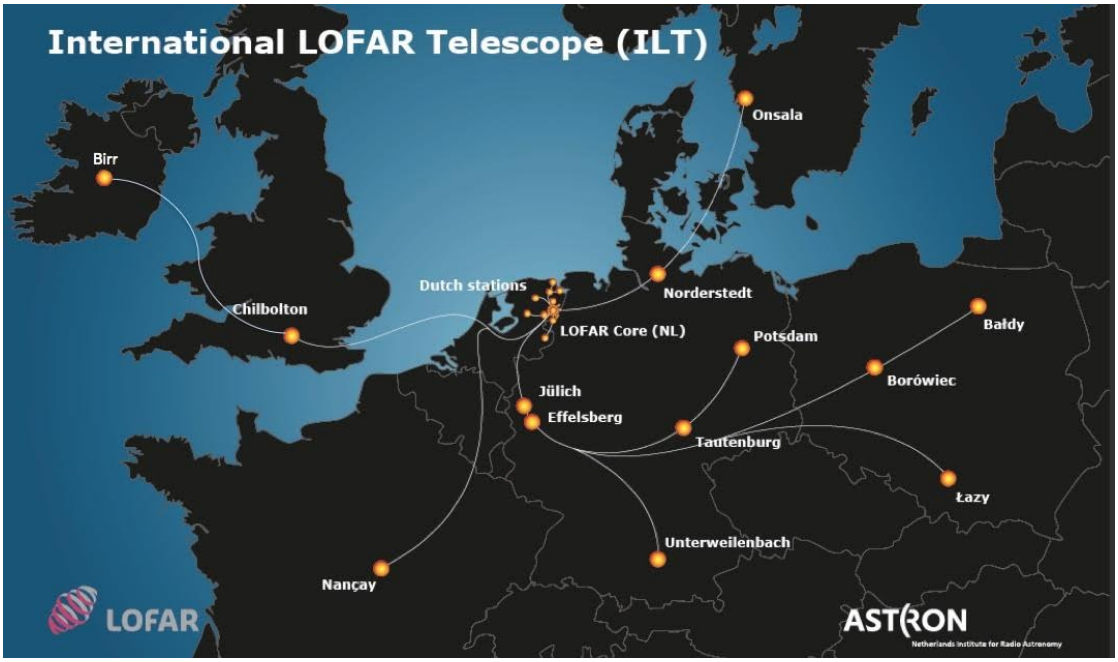

Figure 1.4: The international LOFAR Telescope is a network of stations spread over Europe. Currently there are 38 stations in the Netherlands, six in Germany, three in Poland, and one each in France, Sweden, and the United Kingdom. Another station is currently under construction at Birr Castle in Ireland which will further extend the capabilities of the array.

capabilities, such as being able to observe in many directions simultaneously. However, new technology also provides new challenges, such as very large data volumes and unusual antenna reception patterns. In papers II and III in this thesis we use the part of LOFAR called the High-Band Antenna (HBA) arrays, which can observe in the range 110-240 MHz, to obtain subarcsecond resolution images of the sky. Further details on the calibration and imaging strategies used in this work can be found in Chapter 2 and papers II and III.

Chapter 2

Calibration of interferometric data

This thesis rests on interferometry as an observational technique. In this chapter I summarise a few concepts important for this thesis work, especially for the efforts to calibrate and image data from the international LOFAR telescope. The subject of interferometry is vast and is challenging to convey in a brief and clear way. For questions beyond the scope of this chapter I refer the interested reader to one of the excellent textbooks available on the subject, for example Taylor et al. (1999) and Thompson et al. (2001).

2.1 Long baseline interferometry

The words *long baseline* are frequently used when discussion interferometric observations. There is, however, no easy way to define how long a baseline between two antennas has to be considered *long* and therefore confusion sometimes arise. For example, some people refer to the *remote* Dutch LOFAR stations as having long baselines to the LOFAR core, while others working with international LOFAR stations consider all baselines within the Netherlands to be relatively short. Sometimes one tries to clarify this by using *international* or *intercontinental* to emphasise the really long baselines. However, we note that the longest (national) baseline in the Very Long Baseline Array (VLBA) in the U.S.A. exceeds 8 000 km (Mauna Kea, Hawaii to St. Croix, Virgin Islands), i.e. much longer than the longest (international) LOFAR baseline. The use of short, long and sometimes Very Long (as in the acronym VLBA) is not always obvious, so one has to pay attention to the context to avoid confusion. What is often meant with the phrase *long baselines* is that they may be used to obtain information of celestial objects at relatively high angular resolution.
Other things common to long baseline observations can be the following items:

- Because of the Earth's curvature, all antennas in the array may not see the source at the same time. This requires careful planning of the observations to maximise efficiency.
- The antennas rely on separate time keeping devices, usually atomic clocks. Although stable by everyday standards, the relative drifts of the clocks may introduce significant non-geometric time-variable delays between the antennas which affects the observations. This has to be corrected for in software before e.g. making images of the sky.
- The movement of the antennas, e.g. due to continental drift or land rise, will change the baseline length and orientation. This can to some degree be modelled and corrected for when correlating the measured signals from the antennas, but significant residuals may remain depending on the accuracy of the correlator model. This model also takes into account effects such as time dilation described by the general theory of relativity.
- The sight lines from the antennas may go through very different atmospheric conditions, which affect the propagation of celestial radio waves. This is particularly significant at low (MHz) frequencies where the charged particles in the ionosphere delays the propagating waves in a frequency dependent (dispersive) way.
- Many celestial sources are weaker and have a more complex morphology when observed with long baselines, because of the sensitivity to small angular scales. This can make it challenging to correct for some of the above effects due to the detailed source models needed in some calibration strategies.

All these effects has to be accounted for in some way to extract celestial information from long baseline observations. Fortunately this is possible for many observations, often using calibration schemes which rely on the *triple product* (or closure phase) observable as described by Jennison (1958). However, significant efforts are often required to make images of weak and complex sources.

2.2 The small field-of-view approximation

When the field of view is small enough to ignore the curvature of the celestial sphere, the relation between the measured *visibility* $V(u,v)$, the true sky brightness $I(l,m)$, and the antenna reception pattern $A(l,m)$ (often called *primary beam*) can, in the absence of e.g. atmospheric disturbances, be written as a two dimensional Fourier transform

$$V(u,v) = \int_{-\infty}^{\infty}\int_{-\infty}^{\infty} A(l,m)I(l,m)e^{-2\pi i(ul+vm)} \tag{2.1}$$

where l, m are the sines of the angular separations of the pixels in the image with respect to the phase centre (Taylor et al. 1999, Chap. 2). The parameters u and v are the projected east-west and North-South components of antenna baselines measured in wavelengths, defining a *uv-plane* also referred to as *Fourier space*. The *visibilities* $V(u, v)$ are samples of the Fourier transform of the image, measured by correlating the signals between pairs of stations separated by u and v wavelengths in directions North-South and East-West respectively. Remembering that for small angles $sin(\theta) \approx \theta$ we see that a point source (Dirac delta function) in the image at angular distance l radians from the phase centre will transform to a plane wave in Fourier space with wavelength $1/l$. The larger offset l in the image, the shorter wavelength in Fourier space. Because of rotational invariance of the Fourier transform, the plane wave will have the same direction as a vector pointing from the phase centre to the displaced point source in the image.

2.2.1 Time and frequency smearing

Time and frequency smearing refers to averaging of visibilities in time and frequency respectively. As explained in appendix A, the amount of smearing depends on the distance to the visibility phase centre. A source in the centre is in principle not affected at all, while a source far out may be severely distorted both in shape and flux density.
Following appendix A we estimate that a source at $80''$ distance from the phase centre observed with a 1000 km LOFAR baseline at 150 MHz (2 m wavelength) averaged to 1 channel per LOFAR sub-band (where one sub-band is 195 kHz wide) would suffer a 10% reduction in visibility amplitude due to frequency smearing. This means that sources inside this radius can be imaged with 1000 km baselines without significant distortions, while sources far outside this radius are significantly reduced which simplifies calibration and imaging of complex fields.
Following appendix A we may also obtain an approximate estimate of the amplitude reduction due to time smearing. For a LOFAR observation with $b = 1000$ km and averaging time of 10 seconds, a source at $140''$ distance from the phase centre would suffer a 10% visibility amplitude reduction due to time smearing. We note that in reality, the projected rotational speed of the Earth is less than the approximate value of ω given above since most objects are observed far from the celestial poles, and hence the above estimate should be considered an upper limit.
We further note that in a real data set a range of baseline lengths are present. Therefore, any averaging done using the same averaging kernel (e.g. the same time resolution in seconds) will have a different effect on baselines of different lengths. This means that source structure, such as sizes, may be affected, and

point sources far from the phase centre may appear resolved. In this work, we have assumed a conservative approach and kept the data with high enough time and frequency resolution for smearing to be negligible over the fields imaged.

2.3 Phase-referencing

In principle, interferometers measure the absolute phase difference between signals received at the participating telescopes. However, in practice, the waves are often delayed by e.g. atmospheric turbulence or non-ideal station clocks and electronics. To correct for such effects, which are most significant in long baseline observations, the telescopes often observe, in addition to the target source, one or more calibrator sources with known position and structure. Such a source is usually called a phase calibrator. To track phase variations over time this source is usually monitored throughout the experiment. Afterwards, phase corrections are derived based on the fluctuations observed for the phase calibrator, and these are also applied to the target source. This strategy is called *phase-referencing*.

2.3.1 Phase-referencing in cm-VLBI

Since dish antennas, normally used in global VLBI experiments, usually cannot see both the target and phase calibrator within the primary beam, the antennas must slew between the target and calibrator sources with some cycle time. The time needed on the calibrator sources depends on the source brightness and antenna sensitivity. For the (interpolated) phase reference corrections derived on the calibrator to be valid for the target, the cycle time should be short and therefore the calibrator should be nearby (see e.g. Martí-Vidal et al. 2010). However, if the calibrator is weak, or the telescopes are slow to move, longer time is needed to determine accurate phase corrections. For cm-VLBI, the coherence time of the atmosphere (i.e. the maximum cycle time) is usually a few minutes, which is enough time to slew to a nearby calibrator. This kind of phase-referencing is normally used in global VLBI, and also in observations with the VLA and e-MERLIN arrays described in Sect. 1.4. Still, the need for phase-reference observations significantly limits the observing time on the target source, which limits e.g. the final image sensitivity and thus the scientific interpretation of the observations. However, at centimetre wavelengths the delay is mostly non-dispersive (i.e. independent of frequency) and therefore a wide bandwidth can be used to gain enough signal to noise for a simple linear fit to the residual delays present in the data.

2.3.2 Phase-referencing in metre-VLBI with LOFAR

LOFAR is different from cm-VLBI in that it offers multiple simultaneous pointing directions, without any need for slewing. This makes it possible to observe both target and calibrators simultaneously with continuous tracking of phase changes. This strategy was employed in paper II, where phase corrections were derived for M 82 based on simultaneous observations of the two sources J0957+6533 and M 81. This effort relied on that J0957+6533 was bright enough to divide the observed bandwidth in small chunks of a few MHz each, wherein the dispersive delay (non-linear phase vs frequency) could be approximated as linear and thus solved for using standard cm-VLBI methods (e.g. FRING in AIPS).

While good calibrators can almost always be found within a few degrees at cm-wavelengths, at metre wavelengths the isoplanatic patch (i.e. the area with similar effect on the celestial waves) size seems to be smaller (about 1°). Furthermore, the density of good calibrator sources (with enough flux density in compact structure) is not known at metre wavelengths (Moldón et al. 2015). Ongoing efforts will however greatly increase the numbers of good calibrators, which should simplify future observations of targets all over the northern hemisphere (Jackson et al. 2016). Future fringe-fitting software with capabilities for simultaneous fitting of dispersive and non-dispersive phase errors will also improve the situation since more bandwidth can be used to determine the phase corrections, which in turn enables weaker calibrator sources to be used.

2.4 Flux density calibration

For interferometers with relatively short baselines, such as the VLA described in Sect. 1.4.1, the absolute flux density scale is usually fixed by including a few minutes of observations on a source with known flux density. Because of large number of similar antennas (and the limited angular resolution compared to e.g. VLBI), it is straightforward to determine gain corrections for all antennas based on the observed signal strength towards the calibrator. Good flux density calibrators have been carefully studied for many years and found to be bright and stable over time.

Similar methods are used to calibrate e-MERLIN data, although the small spatial scales sampled by the array require source models for the flux density calibrators to account for resolution effects (i.e. structure in the calibrator source). Indeed, for some calibrator sources, this is important to do also for the VLA.

2.4.1 Flux density calibration in global VLBI

For global VLBI observations it is very challenging to find good flux density calibrator sources to calibrate the gains of all antennas. This is partly due to the fact that the participating antennas may be very different, but also because very detailed models of celestial sources requires an impractical amount of work to keep up to date (e.g. the structure may change more rapidly on smaller scales than larger scales). Instead, the telescope system temperatures (the received power) is monitored during the experiment. Together with measured gain curves (i.e. antenna gain as function of local orientation), a priori amplitude corrections are calculated and applied to the data. Given careful monitoring of the system temperatures and gain curves, this method generally provides flux densities accurate to within 10%.

2.4.2 Flux density calibration in metre-VLBI with LOFAR

International LOFAR observations probe small angular scales where there are few reliable models of flux density calibrators available. Furthermore, measurements of system temperature are not yet performed in a way similar to cm-VLBI. Therefore, it appears as none of the two standard methods described above for short or long baseline interferometry can be used to calibrate flux densities of international LOFAR stations. Accurate flux density calibration is however essential for most scientific interpretations of the data. Fortunately it is possible to employ a modified version of the strategy using sources with known absolute flux density. This strategy has also been used for VLA observations and is commonly referred to as *bootstrapping*.
Bootstrapping for LOFAR observations makes use of two different calibrator sources. One calibrator must have a known flux density at large angular scale (e.g. 3C196) but no model is needed of the source structure at international baseline resolution. Another (preferably point like) calibrator is also observed, which may have unknown total flux density, as long as it has enough flux density on small angular scales to provide high signal-to-noise amplitude corrections during the whole experiment. In paper II this source is J0957+6533, and in paper III we use J1513+2338. Note that, in both these papers, these sources also serve the dual purpose of being delay-calibrators to remove the major residual phase errors towards the target.
To find the correct flux density for our target through bootstrapping, we first assume some flux density for the compact calibrator, for example 0.5 Jy for J0957+6533. We now derive amplitude corrections for the whole experiment based on this assumption, using only the longest baselines ($> 60\,\mathrm{k}\lambda$ in paper II). Because of the smearing on these long baselines the small field of view approximation (see Sect. 2.2) can be used and we only have to care about the single calibrator source, and not about other bright sources several degrees away (as

is the case if we include also shorter baselines, since LOFAR stations pick up emission from a wide field in the sky). The key point here is that although we are only using long baselines, we are including all stations, i.e. also LOFAR stations within the Netherlands. This means that after applying the corrections, we can make a short-baseline image of the source with known flux density to check our guess. If the flux density measured on the absolute flux density calibrator (e.g. 3C196) is found to be too high or too low after applying these corrections, we make another improved guess based on the measured error and iterate until the measured flux density agrees with the (low-resolution) model. The final corrections are then applied to the target.

The impact of primary beam models

The dipole antennas which make up the LOFAR stations have strong directional gain variations. Various studies have shown that although it is possible to correct for these variations to some extent, the current beam models available for LOFAR have significant limitations, as noted in paper III. Future improvements of these models would greatly benefit not only international baseline observations, but also other projects using LOFAR. Work is ongoing to improve the beam models in the near future.

Chapter 3

Summary of appended papers

In this chapter I provide a brief introduction to the questions studied in each of the five appended papers. I also provide brief summaries of the detailed content in each paper, and describe ongoing and future efforts planned to follow up the work presented in this thesis.

3.1 Introduction to paper I: What is powering NGC 4418?

NGC 4418 (at 34 Mpc) is, despite its relatively dull optical appearance compared to the other two galaxies in Fig. 3.1, a very interesting galaxy to study. Although very bright in the infrared ($L_{\rm IR} > 10^{11} L_{\odot}$; i.e. a LIRG), NGC 4418 has significantly less radio emission than expected from the FIR-radio correlation given its IR luminosity (Yun et al. (2001), see Fig. 1.3 in this thesis). Two main scenarios have been proposed to explain this. Either the galaxy hosts a radio-weak active galactic nucleus (AGN) powering the IR emission, or a very young and compact starburst. A mix between the two is also possible (Roche et al. 1986).
Unfortunately, NGC 4418 is extremely obscured by dust and it is therefore very hard to study the nucleus at optical wavelengths. Optical spectroscopy could otherwise prove the existence of a young starburst by for example detecting spectral signatures of young massive Wolf-Rayet stars, as described by Armus et al. (1988).
X-ray observations would also be useful to probe the nucleus of NGC 4418. However, such measurements are inconclusive (Maiolino et al. 2003) since the nucleus is *Compton thick*. Indeed, the column density towards the nucleus is estimated to be $\mathrm{N}_H > 10^{25}\mathrm{cm}^{-2}$ (González-Alfonso et al. 2012).
Although the centre of the galaxy is obscured from optical and X-ray observations, it is possible to map the centre at radio and mm wavelengths. Using mm continuum observations, Sakamoto et al. (2013) found that the central IR power source has an angular size of less than 0.1″. Therefore, to make sharp enough

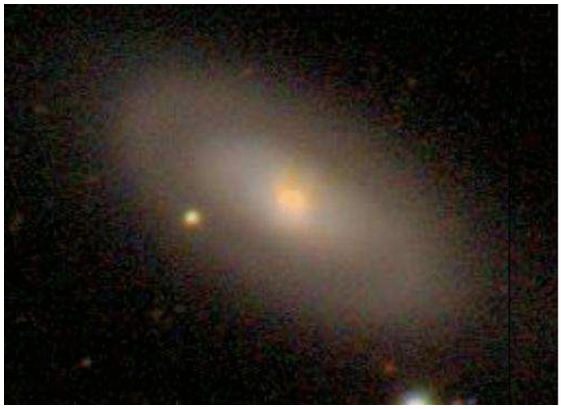

(a)

(b)

(c)

Figure 3.1: Optical images of the three galaxies studied in this thesis: NGC 4418 (Fig. (a), Credit: Sakamoto et al. 2013), M 82 (Fig. (b), Credit: Mutchler et al. 2007), and Arp 220 (Fig. (c), Credit: R. Thompson (U. Arizona) et al., NICMOS, HST, NASA). Note that Fig. (b) is rotated 50° with north approximately towards the top left corner. These are beautiful images, but to see the very smallest details like the supernovae and to see through the obscured central regions with high resolution, we need to use radio or mm wave interferometry.

images of NGC 4418 at cm wavelengths, we need to use very long baseline interferometry.

3.1.1 Summary of paper I

NGC 4418 was observed as a joint EVN and MERLIN project in 2001, but only the (low-resolution) MERLIN part of those data had been previously published (Costagliola et al. 2013). To investigate the structure of the compact radio emission in centre of NGC 4418, we decided to calibrate and image also the EVN data. In paper I we present a combined EVN+MERLIN image of the centre of NGC 4418 with angular resolution 20.6 mas$\times$14.8 mas at 5 GHz (Fig. 2 in paper I). This image for the first time reveals a complex structure in the form of eight compact components. The complexity of this structure is a strong argument against *only* an AGN being present; there must also be a significant contribution from some other emission source, such as intense star formation in the form of massive star clusters.

Sakamoto et al. (2013) estimate that any star formation component must be younger than 30 Myr to explain the faint radio emission. However, we expect even a young starburst to have a steep spectrum typical for synchrotron emission from supernovae ($S_\nu \propto \nu^{-0.8}$, see Sect. 1.2.2). But, when we compare the flux densities measured in compact structure at 1.4 GHz and 5 GHz we see the opposite, i.e. more emission at 5 GHz. To explain this, we model the emission as a well-mixed thermal/non-thermal plasma as suggested by Condon et al. (1991). In this model the synchrotron spectrum is modified at low frequencies by thermal (free-free) absorption.

We obtain a relation between the observed radio surface brightness and star formation rate surface density, by coupling the turnover frequency in the model of Condon et al. (1991) to the SFR via the luminosity-SFR relation of Bell (2003), see Fig. 5 in paper I. For rates of star formation per unit area below $10^3 M_\odot$ yr^{-1}kpc^{-2} free-free absorption is not significant at 5 GHz. But, from the measured surface brightness of NGC 4418, we find that free-free absorption should be significant also at 5 GHz. This would naturally explain the shape of the spectrum and also the lack of radio emission at 1.4 GHz.

Correcting for the possible absorption we estimate a star formation rate surface density of 7-70$M_\odot$ yr^{-1}kpc^{-2}, in good agreement with the 30-100$M_\odot$ yr^{-1}kpc^{-2} estimated by Sakamoto et al. (2013). We conclude that although we do not find strong evidence for or against an AGN, a significant fraction of the radio emission likely comes from a compact starburst in the centre of the galaxy. Some of the compact features we see are likely evidence for intense star formation in the form of massive $10^7 M_\odot$ super star clusters.

3.1.2 Follow-up work

To find out which (if any) of the compact features we see is associated with an AGN we need better image fidelity and more spectral information. Therefore we applied for new observations with the EVN and e-MERLIN telescopes, which were granted and carried out in February and March 2014. One aim of these observations is to get higher sensitivity and better overall image quality at 5 GHz using the improved capabilities of the EVN and e-MERLIN compared to the data from 2001. Another aim was to obtain a high-resolution image also at 1.4 GHz to constrain the spectral index of the compact features. Unfortunately we have not yet had time to look at these data in detail. A preliminary analysis however indicates that we clearly detect NGC 4418 at 5 GHz and that there is a weak signal also at 1.4 GHz with the EVN. This is promising, and will hopefully make it possible to obtain spectral indices for the compact features imaged in paper I.
Given the young age of the starburst in the centre of NGC 4418 one may ask what triggered this activity. In some galaxies, intense star formation is thought to be triggered by interactions with other nearby galaxies, possibly resulting in a merger such as in Arp 220. If NGC 4418 is in an early merger stage, it could be possible to find evidence for this interaction by observations of atomic hydrogen line emission and absorption on arcminute scales. This is the topic of paper V as described in Sect. 3.5.

3.2 Introduction to paper II: Subarcsecond imaging of M 82 with LOFAR

M 82, Fig. 3.1(b), is a nearby (3.6 Mpc) starburst galaxy which has been extensively studied across the electromagnetic spectrum. This galaxy follows the FIR-radio correlation as expected for star forming galaxies (see Fig. 1.3). Its relatively small distance allows detailed studies of star formation physics, e.g. through monitoring of the evolution of supernovae as they interact with their surrounding CSM and ISM. Indeed, monitoring of M 82 since the 1980s has revealed more than 50 compact objects thought to be either synchrotron emitting supernova shocks or free-free emitting HII-regions (Gendre et al. 2013). There is also bright extended emission surrounding the compact sources, visible for example in the natural weighted image of Wills et al. (1997).
One way to study the evolution of the compact objects and their interaction with the surrounding medium is to observe the galaxy at metre wavelengths. At these long wavelengths, the effects of internal (within the compact sources) and external (from the surrounding medium, or foreground) free-free absorption are much more significant than at shorter wavelengths. Also, measurements

of the brightness of supernovae at metre wavelengths help to constrain their evolution, and thereby e.g. the mass-loss histories of the progenitor stars.
To study in detail the compact sources in M 82 at metre wavelengths we require subarcsecond resolution images. Although M 82 has been studied at metre wavelengths before, no instrument was available that could obtain images with sufficient angular resolution to resolve the compact sources. Early commissioning results with the international baselines of LOFAR were however promising (Wucknitz 2010a,b), although no subarcsecond image had been published using the full capabilities of the array.
Combining our interest in technical development with our interest in the physics of star formation, we applied for international LOFAR observations of M 82. The purpose was hence twofold: first to demonstrate that subarcsecond imaging was possible at MHz frequencies using international LOFAR baselines, and second to study the central starburst in M 82 using the new images.

3.2.1 Summary of paper II

Using the international LOFAR telescope we obtained subarcsecond resolution images of M 82 at 118 MHz and 154 MHz (Fig 2. in paper II). The 154 MHz image obtained using international LOFAR baselines is a new record in terms of combined image resolution (0.3″) and sensitivity (0.15 mJy/beam) at low frequencies (< 327 MHz).
We detect 16 objects at 154 MHz with six detected also at 118 MHz. Of the objects seen also at higher frequencies, some show a straight power-law spectrum without clear free-free absorption (Fig. 5 in paper II) while others show a clear low-frequency turnover, indicating significant absorption of the intrinsic synchrotron emission (Fig. 6 in paper II). Seven objects have not previously been reported at higher frequencies, which most likely indicates they have very steep radio spectra. We do not detect any emission from the supernova SN2008iz, which indicate significant absorption effects in this object, see also Kimani et al. (2016).
Most compact sources are located in the star forming disk, although we see no clear spatial correlation of the sources with and without a low-frequency turnover (Fig. 3 in paper II). This can be explained by the sources being randomly situated at different depth along the line of sight within the free-free absorbing disk.
In addition to compact sources we also detect bright extended emission which is most intense immediately above and below the star forming disk in M 82 (Fig. 3 in paper II). We interpret this as the base of the large scale outflow seen e.g. with the HST in Fig. 3.1(b).
Because of the novelty of these data, a lot of effort was required to develop and test a calibration and imaging strategy for data from international LOFAR

baselines, and indeed the description of these efforts is a major part of paper II. We show how a multi-beam approach can be used to obtain noise-limited phase-referenced subarcsecond resolution images with LOFAR by using VLBI techniques in the small-field regime. Our success with M 82 is very promising for future studies of other objects which require similar resolution and sensitivity.

3.2.2 Follow-up work

Building upon the experience from our M 82 observations, we have been involved in multiple other projects using international LOFAR baselines. The most mature project is our observations of Arp 220, which are described in paper III, but we are also involved in ongoing international LOFAR studies of e.g. the galaxy Arp 299. However, although we did a brief analysis of M 82 in paper II, there are still many interesting questions which could be investigated using the M 82 images. For example, we could compare the large-scale radio emission detected with the shorter baselines, see Fig. 3.2 (not discussed in the paper), with observations at 327 MHz with VLA-PT and 408 MHz with MERLIN to study the spectra and absorption of the diffuse emission. Another possibility is to model the spectra of the 50 compact sources, taking into account the measurements or upper limits reported in paper II at 118 MHz and 154 MHz.

3.3 Introduction to paper III: Subarcsecond imaging of Arp 220 with LOFAR

Arp 220, Fig. 3.1(c), is the closest (77 Mpc) ULIRG and has been extensively studied across the electromagnetic spectrum. It is a late-stage merger, which explains the peculiar morphology noted by Arp (1966). The centre is heavily obscured in optical wavelenghts, but radio observations reveal two bright sources about 1″ (370 pc) apart, thought to be the nuclei of two merging galaxies (Norris 1988). Dozens of supernovae and supernova remnants have been detected in the nuclei using cm-VLBI (e.g. Smith et al. 1998; Batejat et al. 2011), consistent with a high SFR (150-300 $M_{\odot}$; Bressan et al. 2002). This makes Arp 220 an excellent laboratory for studies of star formation in extreme environments.
Yun et al. (2001) find Arp 220 marginally fainter at 1.4 GHz than expected from the FIR-radio correlation for star forming galaxies, but within the typical scatter of the correlation, see Fig. 1.3. In the case of Arp 220, the slight deficit in radio emission could be explained if the synchrotron emission from the nuclei is significantly reduced by thermal (free-free) absorption at GHz frequencies. Since this effect is most prominent at lower frequencies (see e.g. Condon 1992), observations at MHz frequencies may constrain the properties and structure of

the absorbing medium.

Although Arp 220 has been observed at MHz frequencies before (Sopp & Alexander 1991; Waldram et al. 1996; Douglas et al. 1996), none of those studies resolved the galaxy. Building upon our successful M 82 observations we decided to observe also Arp 220 using similar techniques to investigate its radio morphology at metre wavelengths. Two main goals were to study the free-free absorption in the two nuclei, and to look for steep spectrum emission undetected at higher frequencies.

3.3.1 Summary of paper III

In paper III we present an image of Arp 220 at 150 MHz with resolution $0.65'' \times 0.35''$ and sensitivity 0.15 mJy/beam, i.e. similar to what we obtained for M 82. We see two emission peaks associated with the two nuclei, embedded in extended radio emission with lower surface brightness. The extended emission was not previously known in the literature. To investigate the nature of the detected radio emission we use archival data from VLA and MERLIN at 1.4 GHz as well as previously published VLA images at 6 and 33 GHz to model the resolved radio spectrum from 150 MHz to 33 GHz.

We find that the two nuclei are significantly affected by free-free absorption, as expected, although the thermal fractions in both nuclei are lower ($< 1\%$) than in many other galaxies. We also find evidence for outflows in both nuclei, consistent with other studies.

We find that the extended emission has a steep spectrum typical for optically thin synchrotron emission, and that it traces the molecular disk surrounding the two nuclei known from e.g. CO(1-0) observations. We argue that the extended radio emission may come from star formation in this disk, and that it is connected to the base of the superwind seen at kpc-scales in the optical.

We find that a simple three component model can explain the observed spectrum of the galaxy. In this model, the nuclei follow the model of Condon et al. (1991) for a well mixed synchrotron free-free plasma (as was the case for NGC 4418 in paper I, but now with lower thermal fractions) while the surrounding extended emission is represented by a sphere of synchrotron emission, where the surface brightness is so low that free-free absorption effects are not significant.

Similar to our study of M 82, this paper shows that LOFAR has great potential to study new components of steep-spectrum emission, such as synchrotron emission from outflows. We note that future studies of LIRGs at MHz frequencies with LOFAR would benefit from using the international LOFAR baselines to resolve the star forming structure.

3.3.2 Follow-up work

Building on this work we want to observe other similar galaxies, i.e. nearby (U)LIRGS, to study free-free absorption and trace steep-spectrum outflows. Observations of the interacting galaxy Arp 299 were carried out during spring 2016 and are presently being analysed by our collaborators. Our experience obtained during the Arp 220 observations have been useful to optimise the observing and data reduction strategy for multiple future international LOFAR observations. The work in this paper is also useful for other studies of Arp 220, such as VLBI-observations trying to connect the population of compact supernova remnants to the smooth radio emission observed from the nuclei. Indeed, this is one aim of the work presented in paper IV.

3.4 Introduction to paper IV: 17 years of VLBI monitoring of Arp 220

As described in Sect. 3.3, Arp 220 is an excellent laboratory in which to study star formation in extreme environments by looking at stellar related radio emission. Radio observations provide the only way to see through the gas and dust obscuring the nuclei at other wavelengths. In paper III we study the synchrotron emission coming from the nuclei of Arp 220 and the effects of thermal absorption on angular scales of $0.3''$. To understand in detail the origin of the radio emission, it is interesting to study the main sources of the accelerated particles which emit the observed synchrotron radiation, i.e. the supernovae and supernova remnants within the two nuclei.

Studies of individual SNe and SNRs in Arp 220 require milliarcsecond resolution, and therefore Arp 220 has been monitored with cm-VLBI since the first detection of the compact sources by Smith et al. (1998). Although previous studies (e.g. Rovilos et al. (2005); Lonsdale et al. (2006); Parra et al. (2007); Batejat et al. (2011)) have gained much insight on the nature of the compact sources, there is still much to be learned from continued monitoring. However, although new single observations may results in higher-quality images than previous studies, there is a lot to be learned also from combining all available data into a self-consistent interpretation. For example, a robust estimate of the rate of very luminous SNe requires multi-frequency observations spanning many years. A robust analysis of the available data requires re-calibration of the archival data, taking into account refinements in e.g. source position since the first observations were made. This is the purpose of paper IV: to analyse, in a self-consistent way, a large amount of cm-VLBI data of Arp 220.

3.4.1 Summary of paper IV

In paper IV we present a self-consistent analysis of new and previously published global VLBI data on Arp 220. We analyse 22 VLBI data sets spanning 17 years and detect 82 compact sources. The spatial distribution of sources trace the star forming disks of the two nuclei seen at lower resolution by e.g. Barcos-Munoz et al. (2015). Most sources are thought to be supernova remnants interacting with the ISM, but about a dozen sources are likely very luminous supernovae interacting with the CSM. We find this consistent with the numbers expected for the rare type IIn, given the total SFR of the galaxy. The sources above our detection threshold follow a luminosity function $n(L) \propto L^{\beta}$ with $\beta = -2.17 \pm 0.16$, similar to normal galaxies.
We also find evidence for a Luminosity-Diameter relation within Arp 220. The observed distribution of source luminosities and sizes is consistent with two underlying populations. One group consists of very luminous SNe where the emitting blast wave is still inside the dense, ionised CSM. The other group consists of less luminous, larger, sources which are thought to be SNRs interacting with the surrounding ISM. The observed number of very luminous SNe is consistent with expectations given a standard initial mass function and the total integrated star formation rate of the galaxy.
Furthermore, we show that the apparent rapid structural variability reported by Batejat et al. (2012) can be explained in terms of beam convolution effects in regions with low surface brightness, rather than intrinsic source structure variabiliy. We also identify the source 0.2227+0.482 as a possible AGN candidate, based on its observed lightcurves, measured size, and centered position in the western nucleus.
When extrapolating the observed luminosity function of compact sources below our detection threshold we find that the population make up at most 25% of the total radio emission from Arp 220 at GHz frequencies. However, secondary CR produced when protons accelerated in the SNRs interact with the dense ISM, and/or re-acceleration of cooled CRs by overlapping SNR shocks, may increase radio emission from the sources below our detection threshold, compared to the extrapolated value. This mechanism may provide enough radio emission to explain the remaining fraction of the radio emission, and could potentially be constrained by future high-sensitivity observations.

3.4.2 Follow-up work

The present paper describes the data and describes the general properties of the population of compact objects. While we only model the multifrequency lightcurves of the brightest object in paper IV, multiple objects are bright enough for similar or more advanced modeling. In a future paper we plan to model, in detail, the evolution of the compact sources. From e.g. lightcurve-fitting

to observed SNe we aim to derive e.g. deceleration parameters and explosion dates. We also aim to constrain the evolution of the progenitor stars through e.g. estimates of mass-loss rates.

We also plan to apply for future multi-frequency monitoring of Arp 220 using global centimetre VLBI observations. Together with the data presented in paper IV, we aim to detect multiple new SNe and to constrain the evolution of the present source population, such as the AGN candidate 0.2227+0.482. We may also detect (through e.g. stacking of new and current sensitive epochs) many more faint sources, which may explain the remaining part of the smooth radio continuum emission in Arp 220. A large low-luminoisity population may further improve our understanding of the physics of the FIR-radio correlation, and quantify the importance of secondary electrons and positrons in dense starbursts.

Finally we note that results from similar ongoing studies of other galaxies, such as the closer LIRG Arp 299 (Perez-Torres et al. in prep.) will be interesting for comparison to the results presented in this work.

3.5 Introduction to paper V: An atomic hydrogen bridge fueling NGC 4418

In this paper we return to the galaxy NGC 4418 which was studied at high spatial resolution in paper I. Redshifted absorption lines has been found towards the nucleus of NGC 4418, including in the mid infrared, OI and OH lines by González-Alfonso et al. (2012) with *Herschel*, and in 21 cm absorption by Costagliola et al. (2013) with MERLIN. These observations indicate infall of molecular and atomic gas. Costagliola et al. (2013) argue that if a central starburst is responsible for all the energy output, it must be 3-10 Myrs old and have a star formation rate $> 10\,\mathrm{M}_{\odot}\ \mathrm{yr}^{-1}$. The complex radio morphology reported in paper I indeed argues in favour of a significant starburst component. If this is the case, an important question is: what triggered this recent starburst in the centre of NGC 4418?

Roche et al. (1986) note that NGC 4418 may be interacting with a nearby galaxy about $3'$ South-East of NGC 4418, i.e. the galaxy VV 655 (also known as MCG+00-32-013). Although the possible companion galaxy is shown by Kawara et al. (1990), their Fig. 1, and mentioned by Evans et al. (2003) and Costagliola et al. (2013), no clear evidence has been presented for any interaction between NGC 4418 and VV 655.

3.5.1 Neutral hydrogen (HI) emission and absorption

One way to find evidence of an interaction scenario is to look for neutral hydrogen tails and debris surrounding NGC 4418. Neutral hydrogen (HI) is the most abundant element in the universe, and can be observed via its hyperfine transition at a wavelength of about 21 cm. HI can be observed both in emission and in absorption (towards a bright background source). In addition to information about the amount of gas present, such observations also probe the velocity structure of the gas through the Doppler shift of the observed spectral lines with respect to the respective rest frequency of HI. In this way, one may get information of how the gas is moving, which may be used to trace e.g. proper motions of interacting galaxies.

3.5.2 Summary of paper V

In paper V we present archival observations of HI taken with the VLA which clearly shows NGC 4418 interacting with the nearby galaxy VV 655. We present spectra and moment maps which indicate that some gas is falling towards the centre of NGC 4418. We conclude that the interaction with VV 655 may very well be what triggered the relatively recent inflow of atomic and molecular gas, and thus the young starburst in NGC 4418.

3.5.3 Follow-up work

The data presented in paper V was taken with the old VLA in its most compact (D) configuration. It would be interesting to re-observe this field with the current (upgraded) VLA, preferably with multiple array configurations, to achieve higher spectral and spatial resolution. With such data it may be possible to study in more detail the velocity structure of HI. In particular it may be possible to get a better understanding of the dynamics and velocity structure of the region closest to NGC 4418.

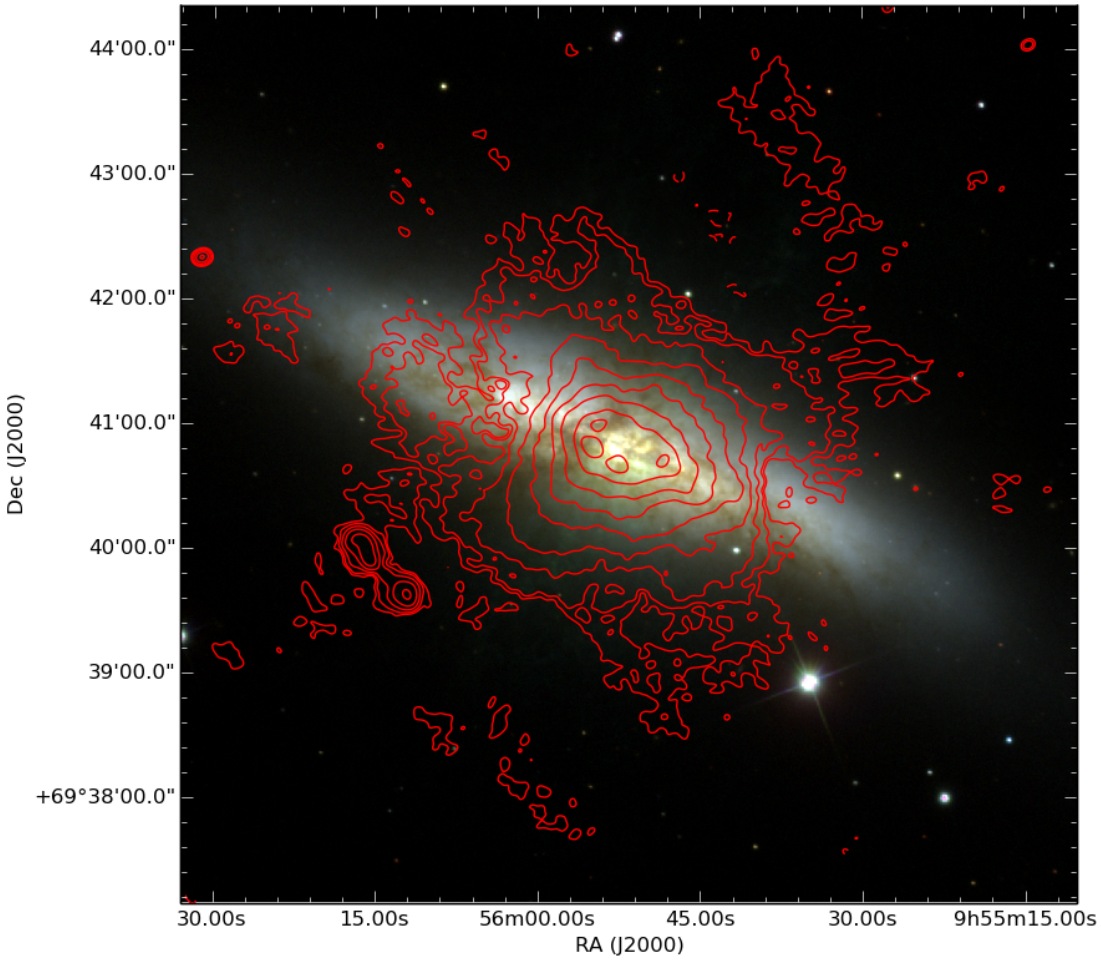

Figure 3.2: Optical SDSS (filters IRG) image of M 82 with 154 MHz LOFAR contours overlayed in red. LOFAR contours at $[-3, 3, 5, 10, 20, 40, 80, 160, 320, 500] \times 0.4\,\mathrm{mJy\,beam^{-1}}$ with resolution $5.7'' \times 4.5''$. Obtained using multiscale CLEAN with baselines in the range 0.1-60 kλ from the data presented in paper II.

Chapter 4

Summary and outlook

In thesis we have studied star formation induced radio emission at metre and centimetre wavelengths on multiple spatial scales. Our groundbreaking images at metre wavelengths have allowed us to study regions tens or hundreds of parsecs in size in the disks of M 82 and Arp 220, where free-free absorption attenuate the synchrotron emission at metre and centimetre wavelengths. We have also studied emission from compact objects in NGC 4418 (of size a few parsec) and in Arp 220 (at subparsec resolution) via centimetre-VLBI observations. These images allow us to study in detail the evolution of supernovae and supernova remnants, which are the sites where the relativistic particles which emit the synchrotron radiation are accelerated, in extreme environments. The sharp images also allow us to search for signatures of AGN activity, although we did not find any clear evidence for this in the three galaxies observed in this thesis. Our observations at metre wavelengths find new steep-spectrum radio components both on pc-scales, i.e. the new compact objects in M 82, and on kpc-scales, i.e. the extended outflows surrounding M 82 and Arp 220.
We find that the observed effects of free-free absorption and steep-spectrum emission may cause significant scatter in the FIR-radio correlation at metre wavelengths, thus reducing its ability to act as a tool for estimates of e.g. star formation rates at these wavelengths. However, on the positive side, metre-wave observations open a new window for studies of topical issues such as galaxy outflows, especially using the high angular resolution provided by international LOFAR baselines. Future studies of other galaxies with subarcsecond resolution at metre wavelengths will likely be very useful to further improve our understanding of the origin of radio emission in star forming galaxies.

Bibliography

Armus, L., Heckman, T. M., & Miley, G. K. 1988, APJL, 326, L45

Arp, H. 1966, ApJS, 14, 1

Barcos-Munoz, L., Leroy, A. K., Evans, A. S., et al. 2015, The Astrophysical Journal, 799, 10

Batejat, F., Conway, J. E., Hurley, R., et al. 2011, ApJ, 740, 95

Batejat, F., Conway, J. E., Rushton, A., et al. 2012, A&A, 542, L24

Bell, E. F. 2003, ApJ, 586, 794

Bracewell, R. N. 1956, Australian Journal of Physics, 9, 198

Bressan, A., Silva, L., & Granato, G. L. 2002, A&A, 392, 377

Condon, J. J. 1992, ARAA, 30, 575

Condon, J. J., Huang, Z.-P., Yin, Q. F., & Thuan, T. X. 1991, ApJ, 378, 65

Costagliola, F., Aalto, S., Sakamoto, K., et al. 2013, AAP, 556, A66

Douglas, J. N., Bash, F. N., Bozyan, F. A., Torrence, G. W., & Wolfe, C. 1996, AJ, 111, 1945

Dreyer, J. L. E. 1888, MmRAS, 49, 1

Evans, A. S., Becklin, E. E., Scoville, N. Z., et al. 2003, AJ, 125, 2341

Gendre, M. A., Fenech, D. M., Beswick, R. J., Muxlow, T. W. B., & Argo, M. K. 2013, MNRAS, 431, 1107

González-Alfonso, E., Fischer, J., Graciá-Carpio, J., et al. 2012, A&A, 541, A4

Heald, G. H., Pizzo, R. F., Orrú, E., et al. 2015, A&A, 582, A123

Jackson, N., Tagore, A., Deller, A., et al. 2016, ArXiv e-prints

Jennison, R. C. 1958, MNRAS, 118, 276

Kawara, K., Taniguchi, Y., Nakai, N., & Sofue, Y. 1990, ApJ, 365, L1

Kennicutt, R. C. & Evans, N. J. 2012, ARA&A, 50, 531

Kimani, N., Sendlinger, K., Brunthaler, A., et al. 2016, ArXiv e-prints

Lacki, B. C., Thompson, T. A., & Quataert, E. 2010, ApJ, 717, 1

Lonsdale, C. J., Diamond, P. J., Thrall, H., Smith, H. E., & Lonsdale, C. J. 2006, ApJ, 647, 185

Maiolino, R., Comastri, A., Gilli, R., et al. 2003, MNRAS, 344, L59

Martí-Vidal, I., Ros, E., Pérez-Torres, M. A., et al. 2010, A&A, 515, A53

Messier, C. 1781, Catalogue des Nébuleuses & des amas d'Étoiles (Catalog of Nebulae and Star Clusters), Tech. rep.

Moldón, J., Deller, A. T., Wucknitz, O., et al. 2015, A&A, 574, A73

Mutchler, M., Bond, H. E., Christian, C. A., et al. 2007, PASP, 119, 1

Norris, R. P. 1988, MNRAS, 230, 345

Parra, R., Conway, J. E., Diamond, P. J., et al. 2007, ApJ, 659, 314

Robitaille, T. P. & Whitney, B. A. 2010, ApJ, 710, L11

Roche, P. F., Aitken, D. K., Smith, C. H., & James, S. D. 1986, MNRAS, 218, 19P

Rovilos, E., Diamond, P. J., Lonsdale, C. J., Smith, H. E., & Lonsdale, C. J. 2005, MNRAS, 359, 827

Sakamoto, K., Aalto, S., Costagliola, F., et al. 2013, APJ, 764, 42

Salim, S., Rich, R. M., Charlot, S., et al. 2007, ApJS, 173, 267

Smith, H. E., Lonsdale, C. J., Lonsdale, C. J., & Diamond, P. J. 1998, ApJ, 493, L17

Sopp, H. M. & Alexander, P. 1991, MNRAS, 251, 112

Taylor, G. B., Carilli, C. L., & Perley, R. A., eds. 1999, Astronomical Society of the Pacific Conference Series, Vol. 180, Synthesis Imaging in Radio Astronomy II

Thompson, A. R., Moran, J. M., & Swenson, G. W. 2001, Interferometry and Synthesis in Radio Astronomy; 2nd ed. (Weinheim: Wiley-VCH)

van Haarlem, M. P., Wise, M. W., Gunst, A. W., et al. 2013, A&A, 556, A2

Waldram, E. M., Yates, J. A., Riley, J. M., & Warner, P. J. 1996, MNRAS, 282, 779

Wills, K. A., Pedlar, A., Muxlow, T. W. B., & Wilkinson, P. N. 1997, MNRAS, 291, 517

Wucknitz, O. 2010a, in 10th European VLBI Network Symposium and EVN Users Meeting: VLBI and the New Generation of Radio Arrays

Wucknitz, O. 2010b, in ISKAF2010 Science Meeting

Yun, M. S., Reddy, N. A., & Condon, J. J. 2001, ApJ, 554, 803

Acronyms

AGN Active Galactic Nucleus.

ALMA The Atacama Large Millimeter/submillimeter Array.

Arp 220 Galaxy number 220 in the *Atlas of peculiar galaxies* by Arp (1966).

CSM Circumstellar material.

EVN The European VLBI Network.

FIR Far infrared.

GHz Gigahertz.

HBA High Band Antenna.

HI Neutral atomic hydrogen.

HII Ionised atomic hydrogen.

HST Hubble Space Telescope.

IRAS The Infrared Astronomical Satellite.

ISM Interstellar medium.

LIRG Luminous Infrared Galaxy.

LOFAR The LOw Frequency ARray.

M 82 Galaxy number 82 in the *Catalog of Nebulae and Star Clusters* by Messier (1781).

MERLIN The Multi-Element Radio Linked Interferometer Network.

MHz Megahertz.

MSSS The LOFAR Multifrequency Snapshot Sky Survey.

NGC 4418 Galaxy number 4418 in the *New General Catalogue of Nebulae and Clusters of Stars* by Dreyer (1888).

NICMOS The Near Infrared Camera and Multi-Object Spectrometer.

SFR Star formation rate.

SKA The Square Kilometre Array.

SNe Supernovae.

SNRs Supernova remnants.

SSA Synchrotron self-absorption.

ULIRG Ultra Luminous Infrared Galaxy.

UV Ultra violet.

VLA The Karl G. Jansky Very Large Array.

VLBA The Very Long Baseline Array.

VLBI Very Long Baseline Interferometry.

Appendices

Appendix A

Time and frequency smearing

Since correlators output a discrete set of visibilities (i.e. samples in time and frequency), averaging is to some extent always done on interferometric data. We may also average the data further after correlation to reduce the computational resources needed for calibration and imaging. Any averaging must however be done with care. Averaging a range of samples in time and frequency together corresponds to averaging over a small parallelogram in Fourier space. This means some information is lost, and one has to take care to not lose information that could affect the scientific results. *Smearing* occurs when the visibilities change significantly in the region (in Fourier space) over which the averaging is done.

A.1 Averaging of plane waves in Fourier space

One way to estimate the effects of averaging is to imagine we have a single point source in our image. If this source is at the phase tracking center, $(l, m) = (0, 0)$, it is not affected by averaging. If however the source is at some offset from the phase center, then its Fourier transform will be a plane wave. If averaging in Fourier space while there is a plane wave present, the amplitude of the plane wave will be reduced. This is called coherence loss or smearing.
A linear slice in any direction through Fourier space containing a plane wave can be described as a sequence of complex numbers. If we assume a linear phase dependence within this sequence (i.e. an ideal wave) we can represent the sequence of numbers as phasors. When averaging along any direction, for example in frequency, the maximum coherence loss will occur if we average in the direction of the plane wave. In the following derivation, we assume maximum coherence loss to estimate the maximum possible effect on the final images.
If we average over a length Δu in Fourier space, we will average all phasors within this length. The phasor angles of the plane wave will cover uniformly

an angle of $\Delta\phi = 2\pi l \Delta u$ (i.e. the fraction of a full period of the plane wave). Since we are only interested in the fractional loss, we can without loss of generality represent the phasors as a set of unit vectors with angles in the range $\pm\Delta\phi/2$.If we average these vectors together, we get one single vector with the average phase 0 (because of our chosen reference) and an amplitude being the normalized sum of all projected amplitudes. The resulting average reduction in amplitude can be written as

$$\frac{I}{I_0} = \frac{\int_{-\Delta\phi/2}^{\Delta\phi/2} \cos(\theta) d\theta}{\int_{-\Delta\phi/2}^{\Delta\phi/2} d\theta} = \frac{\sin(\Delta\phi/2)}{\Delta\phi/2} \tag{A.1}$$

where θ is the phasor angle and cosine is the projection effect when averaging unit vectors. For small changes in phase we can approximate this expression using the first two terms in the Taylor series for the sine function, and we obtain the loss equation

$$\frac{I}{I_0} \approx 1 - \frac{(\pi l \Delta u)^2}{6} \tag{A.2}$$

valid for $l\Delta u \ll 1$, where l is the distance from the phase center (in the image plane) in radians and Δu is the radial length (in the Fourier plane) in units of observing wavelength.

A.2 Frequency smearing

If we average over a frequency range $\Delta\nu$ for a baseline b (in units of observing wavelength), we are summing phasors along a path

$$\Delta u_F = b\Delta\nu/\nu \tag{A.3}$$

where ν is the observing frequency, i.e. the fractional bandwidth times the baseline length. Using $\Delta u = \Delta u_F$ in Eq. A.2 gives an estimate of the frequency smearing on a single baseline of length b.

A.3 Time smearing

An accurate description of time smearing is challenging because the projected baseline length changes with the Earth's rotation. An approximative estimate can however be obtained by approximating the path length in the Fourier plane as the arc

$$\Delta u_T \approx b\Delta t\omega \tag{A.4}$$

where b is the baseline length in units of observing wavelength, Δt is the averaging time, and $\omega \approx 2\pi/(23\text{h}56\text{m})$ is the angular rotation speed of the Earth

around its axis in radians per unit time. Using $\Delta u = \Delta u_T$ in Eq. A.2 gives an estimate of the time smearing on a single baseline of length b.

A.4 Coherence loss due to residual delays and rates

We note that in addition to the purely geometrical effects discussed above, residual phase and delays may be present in the data due to e.g. the ionosphere and imperfect station clocks. These errors may cause visibility amplitudes to be reduced similarly to the above effects for sources far from the phase center.
Residual delays for one antenna means that all baselines related to that antenna have the phase center slightly offset with respect to the desired position. The offset l_τ in radians due to a delay error τ is

$$l_\tau = \arcsin(\tau\nu/u) \tag{A.5}$$

where u is baseline length (in units of observing wavelength) and ν observing frequency (see Chap. 2 in Taylor et al. 1999). Given a certain time and frequency resolution of the data, this offset l_τ may cause significant reduction of visibility amplitudes.
Residual rates will cause the visibility phases to change within the averaging time or frequency interval, even if the source is at the phase center. A residual rate of r mHz (cycles per second) will result in a change of phase within t seconds of $\Delta\phi = r \cdot 10^{-3} \cdot 2\pi \cdot t$ radians.

Paper I

The radio core structure of the luminous infrared galaxy NGC 4418

E. Varenius, J. E. Conway, I. Martí-Vidal, S. Aalto, R. Beswick, F. Costagliola, and H.-R. Klöckner

Astronomy & Astrophysics, 566, 15 (2014).

Paper II

Subarcsecond international LOFAR radio images of the M 82 nucleus at 118 MHz and 154 MHz

E. Varenius, J. E. Conway, I. Martí-Vidal, R. Beswick, A. T. Deller, O. Wucknitz, N. Jackson, B. Adebahr, M. A. Pérez-Torres, K. T. Chyży, T. D. Carozzi, J. Moldón, S. Aalto, R. Beck, P. Best, R.-J. Dettmar, W. van Driel, G. Brunetti, M. Brüggen, M. Haverkorn, G. Heald, C. Horellou, M. J. Jarvis, L. K. Morabito, G. K. Miley, H. J. A. Röttgering, M. C. Toribio, G. J. White

Astronomy & Astrophysics, 574, 114 (2015).

Paper III

Subarcsecond international LOFAR radio images of Arp 220 at 150 MHz. A kpc-scale star forming disk surrounding nuclei with shocked outflows

E. Varenius, J. E. Conway, I. Martí-Vidal, S. Aalto, L. Barcos-Muñoz, S. König, M. A. Pérez-Torres, A. T. Deller, J. Moldón, J. S. Gallagher, T. M. Yoast-Hull, C. Horellou, L. K. Morabito, A. Alberdi, N. Jackson, R. Beswick, T. D. Carozzi, O. Wucknitz, N. Ramírez-Olivencia

Accepted for publication in Astronomy & Astrophysics
DOI: 10.1051/0004-6361/201628702

Paper IV

The population of SNe/SNRs in the starburst galaxy Arp 220. A self-consistent analysis of 17 years of VLBI monitoring.

E. Varenius, F. Batejat, J. E. Conway, I. Martí-Vidal, M. A. Pérez-Torres, S. Aalto, A. Alberdi

Manuscript intended for submission to Astronomy & Astrophysics

Paper V

An atomic hydrogen bridge fueling NGC 4418 with gas from VV 655

E. Varenius, F. Costagliola, H.-R. Klöckner, S. Aalto,H. Spoon, I. Martí-Vidal, J. E. Conway

Manuscript intended for submission to Astronomy & Astrophysics